Ultra-Wideband Photonic Radiometer for Submillimeter Wavelength Remote Sensing

Charles Turner*‡, Mark Stephen*, Fabrizio Gambini†, Gordon Chin*, Paul Racette*, and Thomas Murphy‡,

*NASA Goddard Space Flight Center, Greenbelt, MD, USA

†Integrated Photonics Lab, University of California, Santa Barbara, CA, USA

‡Institute for Research in Electronics and Applied Physics, University of Maryland, College Park, MD, USA

Abstract—The sub-mm wave region of the electromagnetic spectrum, especially the span of 70 GHz centered on the 556.9 GHz H_2O water line, offers a rich harvest of highly diagnostic volatile species that provide powerful insights into a planetary body's origins, thermal history, and conditions for habitability. Previous spaceborne Heterodyne Sub-mm Wave Spectrometers (HSWS) process a small fraction of their capable bandwidth at a given moment. The design of each spectrometer channel also depends on *a priori* knowledge of observable spectral features. Expanding this capability using traditional electronic hardware substantially increases the mass and power consumption of the instrument, limiting its use for CubeSat and SmallSat platforms. Microwave Photonic Integrated Circuits (PIC) is an enabling technology to fabricate an ultra-wideband, high-resolution, sub-mm wave spectrometer that could simultaneously process the receiver's entire bandwidth at a reduced size, weight, and power consumption (SWaP). Through the development of a test platform to combine commercial-off-the-shelf (COTS) and PIC components, we demonstrate the feasibility of a PIC spectrometer.

Index Terms—microwave photonics, photonic integrated circuits, optical filters, remote sensing, radiometer, receiver
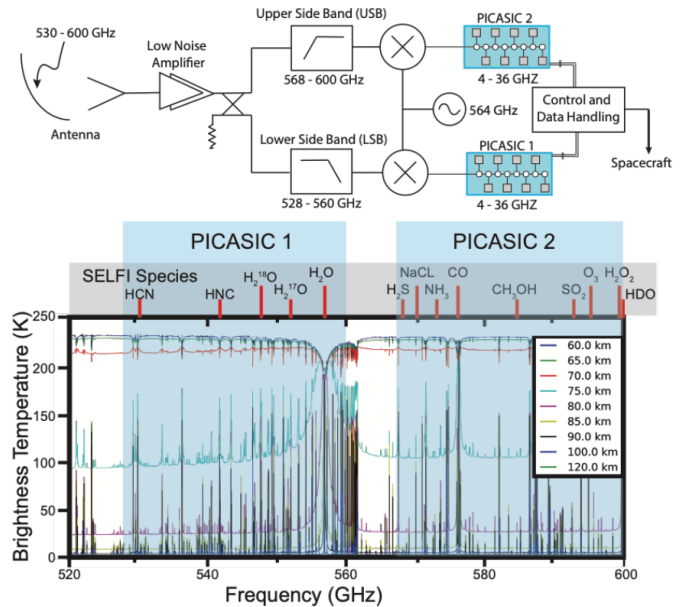
Fig. 1. **Upper:** Instrument block diagram covering the 530-600 GHz spectral region using dual PICASICs to retrieve 128,000 500-kHz resolution channels. This spectral capability measures the spectral line-shapes of numerous compounds that are powerful diagnostics of the chemical composition, pressure, temperature, and dynamics of planetary atmospheres. **Lower:** Simulated Venus atmospheric limb integrations at nine tangent heights (color-coded curves). Blue shaded rectangles show the spectral coverage of dual PICASICs that allow observations of broad and narrow spectral line features and numerous compounds spanning 530–600 GHz. The red vertical lines in the gray shaded box show the frequency peak positions of notable target species

I. INTRODUCTION

We propose leveraging PIC technology to produce a fully-integrated, ultra-wideband (∼70GHz), low-SWaP, Heterodyne Sub-mm Wave Spectrometer (HSWS). Combined with collaborator Pacific Microchip's advances in Application-Specific Integrated Circuit (ASIC) digital spectrometer technology, the instrument will simultaneously resolve the entire bandwidth at a target 0.5 MHz resolution. Radiometers measure noise power emitted from thermal blackbody radiation. Traditional HSWS use a cascade of filters and mixers to down-convert the higher frequencies into narrow, near-baseband channels. This way, these channels can be sampled digitally to achieve the finer resolution necessary to observe either absorption or emission lines from molecular rotating energy transitions [1].

Dividing the sub-mm wave spectrum into channels before the sub-mm wave mixer require the fabrication of filters that are low-yield and expensive, increasing the challenge to accurately fabricate and integrate a large array of channels [2]. This method also requires sub-mm wave mixers for each channel with corresponding sub-mm wave electronic oscillators. Channelizing the spectrum after the sub-mm wave mixer, the intermediate frequency (IF) chain, requires larger filters and additional mixers to down-convert the output of each channel close to baseband with bandwidth suitable for sampling by a digital spectrometer [3]. This is a common system design

for spaceborne HSWS and it either restricts research missions to observe a limited number of molecular species [4] [5] or drives costs for managing a massive, power-hungry behemoth [6]. One work-around is to simply not observe and measure the entire spectrum simultaneously [7].

These options do not meet the requirements for measurements such as the example described in Fig 1. Other research efforts are pursuing similar photonic concepts, such as a microwave spectrometer for earth science applications [8]. This is advantageous where RFI (Radio Frequency Interference) and other factors are challenges that hyperspectral spectroscopy could address [9], but the system has relatively limited bandwidth. The proposed spectrometer is specifically targeting a spaceborne, sub-mm wave Planetary Science ap-
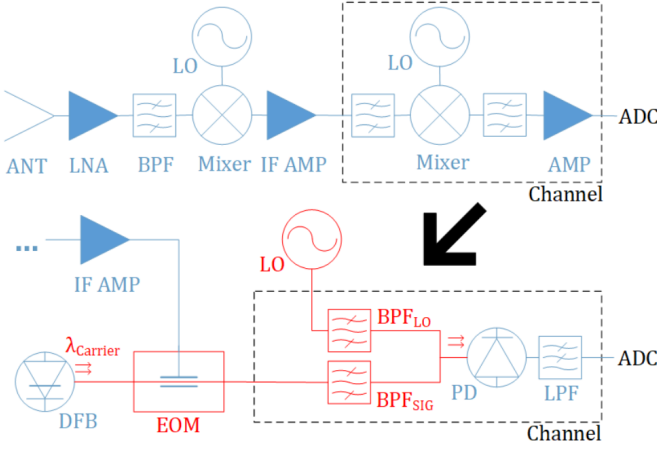
Fig. 2. The HSWS works by measuring noise power from a target source of sub-mm wave (e.g. 530-600 GHz) emissions. The noise power is amplified by a sub-mm wave Low-Noise Amplifier (LNA), which also sets the sensitivity of the receiver. The sub-mm wave power and a tone from a sub-mm wave oscillator are applied to the mixer, which down-converts the spectral information to near baseband (0-70 GHz). Depending on the limitations of the depicted electro-optic modulator (EOM), the spectrum could be split into upper and lower sidebands as depicted in Fig (1) so that each output is more manageable (0-35 GHz). At this stage, the spectrum is split into narrower channels with a bandwidth set by the requirements of the sampling digital spectrometer. **Upper:** Traditional HSWS uses electronic hardware for the IF chain. Each channel filters a portion of the spectrum and requires a mixer and electronic oscillator to down-convert that portion to near baseband (0-4 GHz per channel). The last filter removes the intermodulation products in the channel and amplifies the signal for the digital spectrometer. **Lower:** The proposed HSWS targets the IF chain by integrating the filters, replacing the mixers with photodetectors, and using an optical frequency comb for all the needed oscillator tones on a single PIC [10]. The calibration mechanism is not depicted here, which can vary in design.

plication where RFI is not a significant concern and the entire spectrum needs maximum observation time. In this initial effort, a model is developed for the IF chain of the proposed spectrometer and a single channel is tested using COTS parts to determine the feasibility of leveraging PIC technology in this manner. PIC components have also been developed which will soon be integrated with the system to achieve a more optimal performance. Once the appropriate system design and component technologies are identified, the final step is develop a completely integrated PIC spectrometer.

II. PICASIC RADIOMETER CONCEPT

PICASIC refers to a PIC Spectrometer with connected ASIC digital spectrometers. The overall concept for the PICASIC spectrometer is to simultaneously process the entire receiver bandwidth while eliminating and reducing the SWaP of components in the IF chain. The system is outlined in Fig 2 where the benefits are also illustrated. In areas of the measured spectrum where there are relaxed resolution requirements ($\sim$100 MHz), the intensity at each PIC channel can be measured directly [8]. When a finer resolution is necessary ($\sim$0.5 MHz), the channel can be sampled by a backend digital spectrometer. This eases the bandwidth requirements of the photonic channel ($\sim$4 GHz) and the bin resolution can be adjusted as a trade-off with power consumption. Tunable

optical filters are another feature of PIC technology, an option with no direct counterpart in microwave engineering. This provides an opportunity to reconfigure spectrometers by tuning higher and lower-resolution channels to measure different parts of the spectrum [11]. The result is replacing electronics which cumulatively contain on the order of 10^3 cubic centimeters of volume with a single PIC with dimensions smaller than 10 cubic centimeters. The power consumption of the PIC is predominantly accounted for by the distributed feedback (DFB) laser, which is predicted to be less than, for example, the total power consumption of the IF chain components for a 16-channel HSWS implemented using available microwave components.

III. PERFORMANCE METRICS

At this time, the sensitivity of HSWS is best optimized using state-of-the-art, sub-mm wave, front-end electronics which will be implemented in the proposed design. However, there are promising prospects for eliminating more front-end electronics in the future [12]. Four criteria are identified for comparing traditional spectrometers with the proposed photonic concept.

A. Sensitivity

The system noise and channel bandwidth determine the minimum detectable signal. The dominant contributors of noise in the photonic link (PL) are thermal noise, shot noise, and relative intensity noise (RIN) [13] [14].

$$(PSD)_{thermal,input} = kT \tag{1}$$

$$(PSD)_{thermal,output} = G_{PL}kT \tag{2}$$

$$(PSD)_{shot} = 2qI_{ph}Z_{out} \tag{3}$$

$$(PSD)_{RIN} = 10^{\frac{RIN}{10}}I_{ph}^2 Z_{out} \tag{4}$$

PSD refers to power spectral density, k represents Boltzman's constant, G_{PL} is the gain of the photonic link, T is the system temperature, q is the charge of an electron, I_{ph} is the output photocurrent, and Z_{out} is the load impedance which should typically be matched to 50 Ω. The noise figure (NF) of the system is a measure of all added noise to the input signal.

$$F_{PL} = \frac{S_{out}/N_{out}}{S_{in}/N_{in}} = \frac{(PSD)_{noise}(f)}{GkT} \tag{5}$$

$$F_{PL} = \frac{(1 + G_{PL})kT + 2qI_{ph}Z_{out} + 10^{\frac{RIN}{10}}I_{ph}^2 Z_{out}}{G_{PL}kT} \tag{6}$$

There is an insightful graphical representation available illustrating an approximation of this equation's behavior [13]. As G_{PL} increases to a certain point, the NF decreases towards an optimal shot-noise limited operation. G_{PL} is the output IF to input RF power ratio and is approximated for a single channel by considering a dual-drive MZM with optical filtering

of the RF and LO terms on the upper side-lobe and detection by a balanced photodetector, similar to existing systems [15].

$$\frac{<P_{IF}>}{<P_{RF}>}(f) = \frac{L(f)}{4}\left(\frac{\pi R P_0 J_1\left(\frac{\pi v_{LO}}{v_\pi}\right)}{v_\pi}\right)^2 Z_{in} Z_{out} \quad (7)$$

L consists of the insertion loss in the modulator and LO optical filter, as well as the frequency-dependent loss in the RF optical filter. G_{PL} is improved by increasing the responsivity (R) of the photodetector, the optical power (P_0), tuning the LO voltage (v_{LO}) to its peak value, or reducing the sensitivity of the EOM (v_π). The gain and NF of each component contribute to the final system NF [3]:

$$F_{sys} = F_{LNA} + \frac{F_{PL} - 1}{G_{LNA}} + \frac{F_{BE} - 1}{G_{LNA}G_{PL}} \quad (8)$$

Where F_{BE} is the noise figure of the backend electronics. As long as $G_{LNA} \gg G_{PL}^{-1}$, then $F_{sys} \approx F_{LNA}$.

B. Linear Dynamic Range

The linearity of the proposed system can be characterized using established parameters such as the Second-Order or Third-Order Output Intercept Points (OIP2, OIP3) and the 1 dB power compression point at the input or output of the receiver (IP1, OP1). The Compression Dynamic Range (CDR-1dB) spans from the noise floor to IP1 and must be known to operate the spectrometer in the linear region and minimize calibration errors [16]. The nonlinear behavior of a photonic link is fit by a Bessel function and the IP1 is identified in literature [17].

$$IP1 = \frac{(0.9504 v_\pi)^2}{2\pi^2 Z_{in}} \quad (9)$$

$$CDR_{1dB} = \frac{IP1}{(PSD)_{noise}(f)} \quad (10)$$

The IP1 for a photonic link provides a sufficient upper-limit for linearity. For example, assuming a typical value $V_\pi = 6V$, the IP1 is estimated at 15.2 dBm. At this value, the CDR is more likely limited by the front-end LNA.

C. Selectivity

Selectivity refers to how well a channel can measure a desired noise power. There will be some amount of unwanted power leaked from one channel to another. This is due to channel overlap, phase noise in the oscillators, and the spurious free dynamic range (SFDR).

$$S(f)\,[dB] = C\,[dB] - I\,[dB] - L\,[dB] - B\,[dB] \quad (11)$$

Selectivity (S) is determined by the signal power (C) and unwanted (intereference) noise power (I). L is noise power from the phase noise of the optical carrier or LO and B is the bandwidth of the channel [3]. These factors will cause power to leak into unintended channels.

$$SFDR = \left(\frac{OIP_3}{(PSD)_{noise}(f)}\right)^{(2/3)} \quad (12)$$

SFDR spans the range between the noise floor and the OIP3 of the photonic link [13]. This metric quantifies contributions from spurs that will also mix and generate interference.

D. Stability

Stability is a measure of how long an instrument can continue to measure a source and improve uncertainty in the measurement. Each of the identified noise sources are a result of random fluctuations and stochastic signal theory can be used to describe uncertainty in the measurement [16].

$$\Delta T \approx T_{sys} \left(\frac{1}{B\tau} + \left(\frac{\Delta G}{G}\right)^2\right)^{1/2} \quad (13)$$

The radiometer equation shows that when a digital spectrometer samples a channel for a longer integration period, the uncertainty in the measurement improves. In practice, this is only true for a limited amount of time. Gain fluctuations caused by multiple sources will limit the spectrometer's ability to resolve a measured source. This particular performance criteria will be investigated in a future effort using Allan Variance testing [18].

IV. MEASUREMENTS

The feasibility of the proposed IF channel design was verified through a series of baseline measurements for sensitivity and dynamic range. These measurements were performed on simplified circuits with readily available COTS components and test equipment. The most simple and stable circuit consisted of a Lucent 20 GHz Mach-Zehnder Modulator (MZM). A Fitel 1550 nm DFB laser provided 6.7 dBm optical carrier power. Combined with a Thorlabs InGaAs photodetector, the overall conversion loss was measured at 33.5 dB for a 1 GHz signal. A L3-Harris LNA with 58 dB gain was used to amplify the input RF noise power and overcome losses in the photonic link. A MiniCircuits 4.2 GHz bias-tee provided a
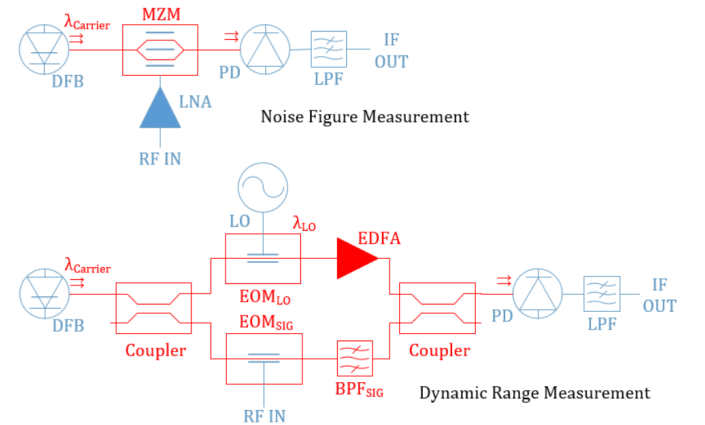

Fig. 3. **Upper:** Microwave photonic radiometer assembled for noise figure measurement containing L3-Harris LNA, Lucent Intensity Modulator (MZM), and Thorlabs InGaAs Photodetector. **Lower:** Tunable radiometer with optical filtering assembled for dynamic range measurements. System includes Thorlabs and JDSU Phase Modulators, IPG Photonics EDFA, Teraxion FBG optical filter, and ThorLabs InGaAs Photodetector.
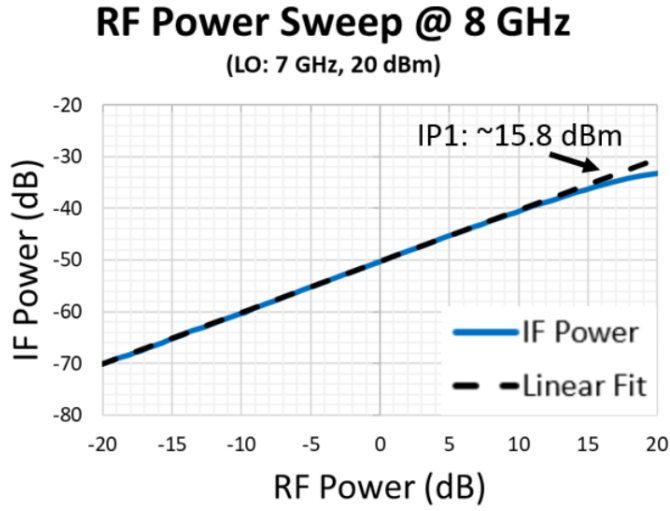
Fig. 4. Plot depicts IF output power versus RF input power for system presented in Fig. 3. The 1 dB compression point at the input (IP1) is measured at 15.8 dBm. This is in close agreement with the theory, as the Thorlabs EOM $v_\pi \approx 6.4$ volts at 8 GHz, leading to a predicted IP1 of 15.7 dBm.

DC path to ground for the photocurrent, as well as a low-pass filter (LPF) for the output. The noise figure of the receiver was measured using the Y-factor method [3]. The input of the receiver was terminated with a 50Ω load measured at both ambient (290K) and cooled (80K) temperatures. In each case, the total integrated power was measured at the output of the receiver using a Boonton RF power meter. This test was performed on the LNA, the photonic link, and the complete system illustrated in Fig. 3. The results are provided in Table I and demonstrate that if the gain of the LNA is large enough to overcome the losses in the photonic link, then the noise figure of the receiver will be set by LNA.

The second circuit is a closer representation of an IF channel in the proposed HSWS and was tested for its functionality and dynamic range. The RF signal (8 GHz) was applied to a Thorlabs 40 GHz phase EOM and passed through a Teraxion 3.5 GHz BW Fiber-Bragg Grating filter. The DFB laser power was split to generate an LO tone with a JDSU 10 GHz phase EOM. This method was used to avoid drift between the LO (7 GHz) and RF side lobes. The LO power was driven high (20 dBm) since the LO side lobe was 3.81 dBc relative to the optical carrier power of -5.30 dBm on that circuit branch. The optical power was amplified using an Erbium-Doped Fiber Amplifier (EDFA) to 10 dBm, but even so, the resulting conversion loss of the photonic link was near 50 dB for an IF output of 1 GHz. By sweeping the RF power, the IP1 of the system was confirmed and the results are presented in Fig 4.

V. SUMMARY

The main objective is to determine the feasibility of the proposed HSWS concept. For this design, we found electronics are the limiting factor for the spectrometer's sensitivity and dynamic range. The next steps include modifying the photonic link to introduce more optical power and improve conversion loss [15] [17]. Once optimized, the noise figure measurement will be repeated on the new setup with an ultra-wideband LNA. Near-term efforts also include investigating channel cross-talk and long-term measurement stability.

REFERENCES

[1] C. K. Walker, *Terahertz Astronomy*. Boca Raton, FL: CRC Press, 2015.
[2] G. Chattopadhyay, T. Reck *et al.*, "Micromachined packaging for terahertz systems," *Proceedings of the IEEE*, vol. 105, no. 6, pp. 1139–1150, 2017.
[3] D. Pozar, *Microwave Engineering, 4th Edition*. Wiley, 2011. [Online]. Available: https://books.google.com/books?id=JegbAAAAQBAJ
[4] G. J. Melnick, A. Dalgarno *et al.*, "The submillimeter wave astronomy satellite: Science objectives and instrument description," *European Space Agency, (Special Publication) ESA SP*, no. 401, pp. 189–194, 1997.
[5] S. Gulkis, M. Frerking *et al.*, "MIRO: Microwave Instrument for Rosetta Orbiter," *Space Science Reviews*, vol. 128, no. 1-4, pp. 561–597, May 2007. [Online]. Available: http://link.springer.com/10.1007/s11214-006-9032-y
[6] J. W. Waters, L. Froidevaux *et al.*, "The Earth Observing System Microwave Limb Sounder (EOS MLS) on the Aura Satellite Walch'Walch'Abstract-EOS MLS measures several atmospheric chemical species (OH," 2006. [Online]. Available: http://mls.jpl.nasa.gov
[7] H. L. Nordh, F. Von Schéele *et al.*, "The Odin orbital observatory," *Astronomy and Astrophysics*, vol. 402, no. 3, 2003.
[8] T. Pett, J. H. Lee *et al.*, "Photonics-based Microwave Radiometer for Hyperspectral Earth Remote Sensing," *MWP 2018 - 2018 International Topical Meeting on Microwave Photonics*, pp. 17–20, 2018.
[9] S. A. Boukabara and K. Garrett, "Benefits of a hyperspectral microwave sensor: Applications in environmental monitoring and weather forecasting," *Proceedings of IEEE Sensors*, pp. 1881–1884, 2011.
[10] P. Marin-Palomo, J. N. Kemal *et al.*, "Microresonator-based solitons for massively parallel coherent optical communications," *Nature*, vol. 546, no. 7657, pp. 274–279, 2017.
[11] J. E. Cunningham, I. Shubin *et al.*, "Highly-efficient thermally-tuned resonant optical filters," *Opt. Express*, vol. 18, no. 18, pp. 19 055–19 063, Aug 2010. [Online]. Available: http://www.opticsexpress.org/abstract.cfm?URI=oe-18-18-19055
[12] M. Burla, C. Hoessbacher *et al.*, "500 GHz plasmonic Mach-Zehnder modulator enabling sub-THz microwave photonics," *APL Photonics*, vol. 4, no. 5, 2019. [Online]. Available: http://dx.doi.org/10.1063/1.5086868
[13] F. Bucholtz, V. J. Urick *et al.*, "Graphical approach for evaluating performance limitations in externally modulated analog photonic links," *IEEE Transactions on Microwave Theory and Techniques*, vol. 56, no. 1, pp. 242–247, 2008.
[14] D. Marpaung, "High dynamic range analog photonic links," Ph.D. dissertation, University of Twente, 2009. [Online]. Available: http://purl.org/utwente/doi/10.3990/1.9789036528603
[15] S. T. Lipkowitz, T. U. Horton, and T. E. Murphy, "Wideband microwave electro-optic image rejection mixer," *Opt. Lett.*, vol. 44, no. 19, pp. 4710–4713, Oct 2019. [Online]. Available: http://ol.osa.org/abstract.cfm?URI=ol-44-19-4710
[16] P. Racette and R. H. Lang, "Radiometer design analysis based upon measurement uncertainty," *Radio Science*, vol. 40, no. 5, pp. 1–22, 2005.
[17] V. Urick, K. Williams, and J. McKinney, *Fundamentals of Microwave Photonics*, ser. Wiley Series in Microwave and Optical Engineering. Wiley, 2015. [Online]. Available: https://books.google.com/books?id=6MQhBgAAQBAJ
[18] S. Stein, "The Allan Variance-Challenges and Opportunities," *IEEE Transactions on Ultrasonics, Ferroelectrics, and Frequency Control*, vol. 57, no. 3, pp. 540–547, 2010.